

000
001
002054
055
056003

External Prior Guided Internal Prior Learning for Real Noisy Image Denoising

057
058004
005
006
007
008
009
010
011059
060
061
062
063
064
065

012 Anonymous CVPR submission

066

013 Paper ID 1047

067

Abstract

Most of existing image denoising methods use some statistical models such as additive white Gaussian noise (AWGN) to model the noise, and learn image priors from either external data or the noisy image itself to remove noise. However, the noise in real-world noisy images is much more complex than AWGN, and it is hard to be modeled by simple analytical distributions. Therefore, many state-of-the-art denoising methods in literature become much less effective when applied to real noisy images. In this paper, we develop a robust denoiser for real noisy image denoising without explicit assumption on noise models. Specifically, we first learn external priors from a set of clean natural images, and then use the learned external priors to guide the learning of internal latent priors from the given noisy image. The proposed method is simple yet highly effective. Experiments on real noisy images demonstrate that it achieves much better denoising performance than state-of-the-art denoising methods, including those designed for real noisy images.

1. Introduction

Image denoising is a crucial and indispensable step to improve image quality in digital imaging systems. In particular, with the decrease of size of CMOS/CCD sensors, noise is more easily to be corrupted and hence denoising is becoming increasingly important for high resolution imaging. In literature of image denoising, the observed noisy image is usually modeled as $\mathbf{y} = \mathbf{x} + \mathbf{n}$, where \mathbf{x} is the latent clean image and \mathbf{n} is the corrupted noise. Numerous image denoising methods [1, 2, 3, 4, 5, 6, 7, 8, 9, 10, 11, 12, 13] have been proposed in the past decades, including sparse representation and dictionary learning based methods [1, 2, 3], nonlocal self-similarity based methods [4, 5, 6, 3, 7], low-rank based methods [8], neural network based methods [9], and discriminative learning based methods [10, 11].

Most of the existing denoising methods [1, 2, 4, 5, 6, 3, 7, 8, 9, 10, 11, 12, 13] mentioned above assume noise \mathbf{n} to be additive white Gaussian noise (AWGN). Unfortunately, this assumption is too ideal to be true for real-world noisy im-

ages, where the noise is much more complex than AWGN [14, 15] and varies by different cameras and camera settings (ISO, shutter speed, and aperture, etc.). According to [15], the noise corrupted in the imaging process [is signal dependent and comes from five main sources: photon shot, fixed pattern, dark current, readout, and quantization noise. As a result, many advanced denoising methods in literature becomes much less effective when applied to real-world noisy images. Fig. 1 shows an example, where we apply some representative and state-of-the-art denoising methods, including CBM3D [6], WNNM [8], MLP [9], CSF [10], and TRD [11], to a real noisy image (captured by a Nikon D800 camera with ISO is 3200) provided in [14]. One can see that these methods either remain the noise or over-smooth the image details on this real noisy image.

There have been a few methods [16, 17, 18, 14, 19, 20, 21] developed for real noisy image denoising. Almost all of these methods follow a two-stage framework: first estimate the parameters of the assumed noise model (usually Gaussian or mixture of Gaussians (MoG)), and then perform denoising with the estimated noise model. Again, the noise in real noisy images is very complex and hard to be modeled by explicit distributions such as Gaussian and MoG. Fig. 1 also shows the denoised results of two state-of-the-art real noisy image denoising methods, Noise Clinic [19, 20] and Neat Image [21]. One can see that these two methods do not perform well on this noisy image either.

This work aims to develop a robust solution for real noisy image denoising without explicitly assuming certain noise models. To achieve this goal, we propose to first learn image priors from external clean images, and then employ the learned external priors to guide the learning of internal latent priors from the given noisy image. The flowchart of the proposed method is illustrated in Fig. 2. We first extract millions of patch groups from a set of high quality natural images, with which a Gaussian Mixture Model (GMM) is learned as the external prior. The learned GMM prior model is used to cluster the patch groups extracted from the given noisy image, and then a hybrid orthogonal dictionary (HOD) is learned as the internal prior for image denoising. Our proposed denoising method is simple and ef-

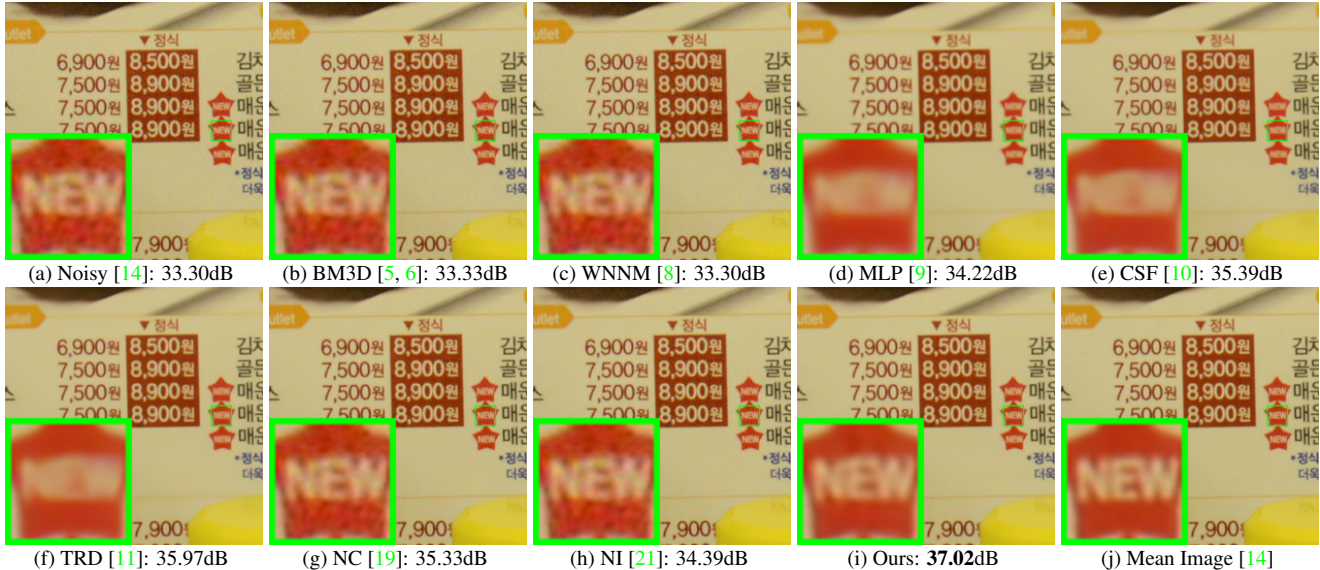


Figure 1. Denoised images of the real noisy image “Nikon D800 ISO 3200 A3” from [14] by different methods. The images are better viewed by zooming in on screen.

ficient, yet our extensive experiments on real noisy images clearly demonstrate its better denoising performance than the current state-of-the-arts.

2. Related Work

2.1. Internal vs. External Prior Learning

Image priors are playing a key role in image denoising [7, 13, 1, 22, 3, 23]. There are mainly two categories of prior learning methods. 1) External prior learning methods [12, 7, 13] learn priors (e.g., dictionaries) from a set of external clean images, and the learned priors are used to recover the latent clean image from noisy images. 2) Internal prior learning methods [1, 3, 22, 23] directly learn priors from the given noisy image, and the image denoising is often done simultaneously with the prior learning process. It has been demonstrated [7, 13] that the external priors learned from natural clean images are effective and efficient for image denoising problem, but they are not adaptive to the given noisy image so that some fine-scale image structures may not be well recovered. By contrast, the internal priors are adaptive to content of the given image, but the learning processing are usually slow. In addition, most of the internal prior learning methods [1, 3, 22, 23] assume AWGN noise, making the learned priors less robust for real noisy images. In this paper, we use external priors to guide the internal prior learning. Our method is not only much faster than the traditional internal learning methods, but also very effective to denoise real noisy images.

2.2. Real Noisy Image Denoising

In the last decade, there are many methods [16, 17, 19, 20, 18, 14] for blind image denoising problem. These meth-

ods can be applied to real noisy image denoising directly. Liu *et al.* [16] proposed to use “noise level function” to estimate the noise and then use Gaussian conditional random field to obtain the latent clean image. Gong et al. [17] models the noise by mixed ℓ_1 and ℓ_2 norms and remove the noise by sparsity prior in the wavelet transform domain. Recently, Zhu et al. proposed a Bayesian model [18] which approximates and removes the noise via low-rank mixture of Gaussians. The method of “Noise Clinic” [19, 20] and the software of Neat Image [21] are developed specifically for real noisy image denoising. “Noise Clinic” [19, 20] generalizes the NL-Bayes model [24] to deal with blind noise and achieves state-of-the-art performance. However, these methods largely depends on the modeling of noise in real noisy images which is hard to be modeled by explicit distributions. Besides, the parametric estimation of the Gaussian or MoG distribution is often time consuming.

3. External Prior Guided Internal Prior Learning

In this section, we first describe the learning of external prior, and then describe in detail the guided internal prior learning. Finally, the denoising algorithm with the learned priors is presented.

3.1. Learn External Patch Group Priors

The nonlocal self-similarity based patch group (PG) [7] has proved to be a very effective unit for image prior learning. In this work, we also extract PGs from natural clean images to learn priors. A PG is a group of similar patches to a local patch.

In our method, each local patch is extracted from a

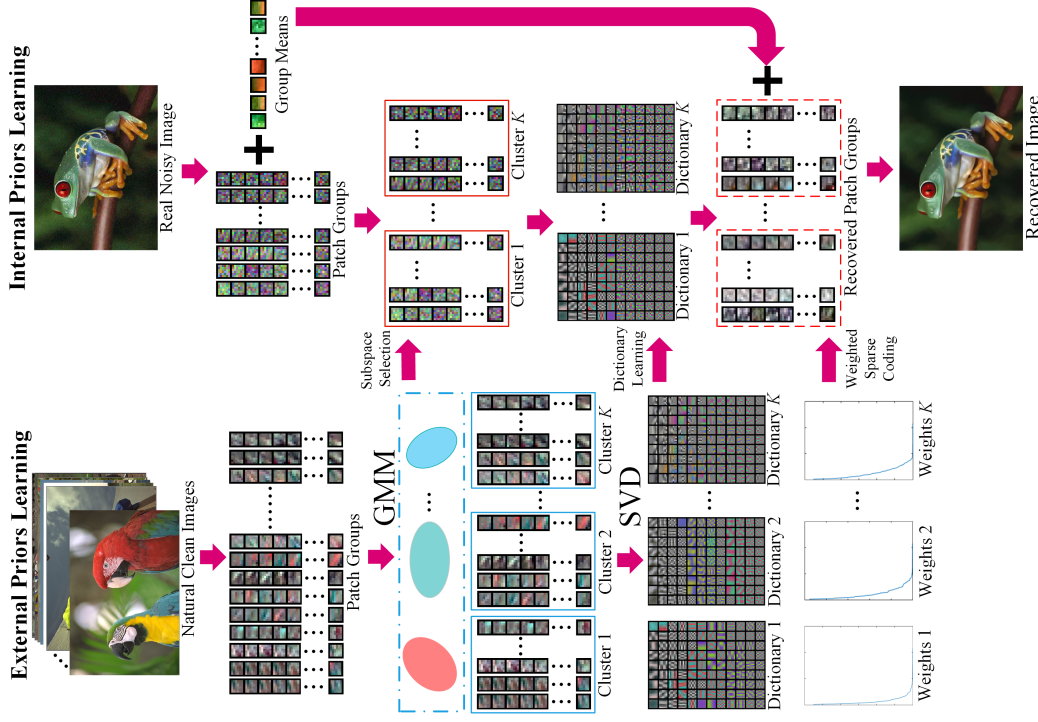


Figure 2. Flowchart of the proposed external prior guided internal prior learning and real noisy image denoising framework.

RGB image with patch size $p \times p \times 3$. We search the M most similar patches to this local patch (including the local patch itself) in a $W \times W$ local region around it. Each patch is stretched to a patch vector $\mathbf{x}_m \in \mathbb{R}^{3p^2 \times 1}$ to form the PG $\{\mathbf{x}_m\}_{m=1}^M$. The mean vector of this PG is $\mu = \frac{1}{M} \sum_{m=1}^M \mathbf{x}_m$, and the group mean subtracted PG is defined as $\bar{\mathbf{X}} \triangleq \{\bar{\mathbf{x}}_m = \mathbf{x}_m - \mu\}$.

Assume we extract a number of N PGs from a set of external natural images, and the n -th PG is $\bar{\mathbf{X}}_n \triangleq \{\bar{\mathbf{x}}_{n,m}\}_{m=1}^M, n = 1, \dots, N$. A Gaussian Mixture Model (GMM) is learned to model the PG prior. The overall log-likelihood function is

$$\ln \mathcal{L} = \sum_{n=1}^N \ln \left(\sum_{k=1}^K \pi_k \prod_{m=1}^M \mathcal{N}(\bar{\mathbf{x}}_{n,m} | \mu_k, \Sigma_k) \right). \quad (1)$$

The learning process is similar to the GMM learning in [7, 13]. Finally, a GMM model with K Gaussian components is learned, and the learned parameters include mixture weights $\{\pi_k\}_{k=1}^K$, mean vectors $\{\mu_k\}_{k=1}^K$, and covariance matrices $\{\Sigma_k\}_{k=1}^K$. Note that the mean vector of each cluster is naturally zero, i.e., $\mu_k = \mathbf{0}$.

To better describe the subspace of each Gaussian component, we perform singular value decomposition (SVD) on the covariance matrix:

$$\Sigma_k = \mathbf{U}_k \mathbf{S}_k \mathbf{U}_k^\top. \quad (2)$$

The eigenvector matrices $\{\mathbf{U}_k\}_{k=1}^K$ will be employed as the external orthogonal dictionary to guide the internal dictionary learning in next sub-section. In Fig. 3 (a) and (b), we

illustrate an external clean image and one orthogonal dictionary learned via GMM on PGs of the external clean image. The singular values in \mathbf{S}_k reflect the significance of the singular vectors in \mathbf{U}_k . They will also be utilized as prior weights for weighted sparse coding in our denoising algorithm.

3.2. Guided Internal Prior Learning

After the external PG prior is learned, we employ it to guide the internal PG prior learning for a given real noisy image. The guidance lies in two aspects. One is that the external prior can guide the subspace assignment of internal noisy PGs, while the other is that the external prior could guide the orthogonal dictionary learning of internal noisy PGs.

3.2.1 Internal Subspace Assignment

Given a real noisy image, we extract N (overlapped) local patches from it. Similar to the external prior learning stage, for the n -th local patch we search its M most similar patches around it to form a noisy PG, denoted by $\mathbf{Y}_n = \{\mathbf{y}_{n,1}, \dots, \mathbf{y}_{n,M}\}$. Then the group mean of \mathbf{Y}_n , denoted by μ_n , is subtracted from each patch by $\bar{\mathbf{y}}_{n,m} = \mathbf{y}_{n,m} - \mu_n$, leading to the mean subtracted noisy PG $\bar{\mathbf{Y}}_n \triangleq \{\bar{\mathbf{y}}_{n,m}\}_{m=1}^M$.

The external GMM prior models $\{\Sigma_k\}_{k=1}^K$ basically characterize the subspaces of natural high quality PGs. Therefore, we project the noisy PG $\bar{\mathbf{Y}}_n$ into the subspaces of $\{\Sigma_k\}_{k=1}^K$ and assign it to the most suitable subspace

324

based on the posterior probability:

$$P(k|\bar{\mathbf{Y}}_n) = \frac{\prod_{m=1}^M \mathcal{N}(\bar{\mathbf{y}}_{n,m}|\mathbf{0}, \Sigma_k)}{\sum_{l=1}^K \prod_{m=1}^M \mathcal{N}(\bar{\mathbf{y}}_{n,m}|\mathbf{0}, \Sigma_l)} \quad (3)$$

for $k = 1, \dots, K$. Then $\bar{\mathbf{Y}}_n$ is assigned to the component with the maximum A-posteriori (MAP) probability $\max_k P(k|\bar{\mathbf{Y}}_n)$.

3.2.2 Guided Orthogonal Dictionary Learning

Assume we have assigned all the internal noisy PGs $\{\bar{\mathbf{Y}}_n\}_{n=1}^N$ to their corresponding most suitable subspaces in $\{\mathcal{N}(\mathbf{0}, \Sigma_k)\}_{k=1}^K$. For the k -th subspace, the noisy PGs assigned to it are $\{\bar{\mathbf{Y}}_{k,n}\}_{n=1}^{N_k}$ where $\bar{\mathbf{Y}}_{k,n} = [\bar{\mathbf{y}}_{k,n,1}, \dots, \bar{\mathbf{y}}_{k,n,M}]$ and $\sum_{k=1}^K N_k = N$. We propose to learn an orthogonal dictionary \mathbf{D}_k from each set of PGs $\bar{\mathbf{Y}}_{k,n}$ with the guidance of the corresponding external orthogonal dictionary \mathbf{U}_k (Eq. (2)) to characterize the internal PG prior. The reasons that we learn orthogonal dictionaries are two-fold. Firstly, the PGs $\bar{\mathbf{Y}}_{k,n}$ are in a subspace of the whole space of all PGs, therefore, there is no necessary to learn a redundant over-complete dictionary to characterize it, while an orthonormal dictionary has naturally zero *mutual incoherence* [25]. Secondly, the orthogonality of dictionary can make the encoding in the testing stage very efficient, leading to an efficient denoising algorithm (please refer to sub-section 3.3 for details).

We let the orthogonal dictionary \mathbf{D}_k be $\mathbf{D}_k \triangleq [\mathbf{D}_{k,E} \ \mathbf{D}_{k,I}] \in \mathbb{R}^{3p^2 \times 3p^2}$, where $\mathbf{D}_{k,E} = \mathbf{U}_k(:, 1:r) \in \mathbb{R}^{3p^2 \times r}$ is the external sub-dictionary and it includes the first r most important eigenvectors of \mathbf{U}_k , and the internal sub-dictionary $\mathbf{D}_{k,I}$ is to be adaptively learned from the noisy PGs $\{\bar{\mathbf{Y}}_{k,n}\}_{n=1}^{N_k}$. The rationale to design \mathbf{D}_k as a hybrid dictionary is as follows. The external sub-dictionary $\mathbf{D}_{k,E}$ is pre-trained from external clean data, and it represents the k -th latent subspace of natural images, which is helpful to reconstruct the common latent structures of images. However, $\mathbf{D}_{k,E}$ is general to all images and it is not adaptive to the given noisy image. Some fine-scale details specific to the given image may not be well characterized by $\mathbf{D}_{k,E}$. Therefore, we learn an internal sub-dictionary $\mathbf{D}_{k,I}$ to supplement $\mathbf{D}_{k,E}$. In other words, $\mathbf{D}_{k,I}$ is to reveal the latent subspace adaptive to the input noisy image, which cannot be effectively represented by $\mathbf{D}_{k,E}$.

For notation simplicity, in the following development we ignore the subspace index k for $\bar{\mathbf{Y}}_{k,n}$ and \mathbf{D}_k , etc. The learning of hybrid orthogonal dictionary \mathbf{D} is performed under the following weighted sparse coding framework:

$$\begin{aligned} & \min_{\mathbf{D}, \{\alpha_{n,m}\}} \sum_{n=1}^N \sum_{m=1}^M (\|\bar{\mathbf{y}}_{n,m} - \mathbf{D}\alpha_{n,m}\|_2^2 + \sum_{j=1}^{3p^2} \lambda_j |\alpha_{n,m,j}|) \\ & \text{s.t. } \mathbf{D} = [\mathbf{D}_E \ \mathbf{D}_I], \mathbf{D}_I^\top \mathbf{D}_I = \mathbf{I}_r, \mathbf{D}_E^\top \mathbf{D}_I = \mathbf{0}, \end{aligned} \quad (4)$$

where $\alpha_{n,m}$ is the sparse coding vector of the m -th patch $\bar{\mathbf{y}}_{n,m}$ in the n -th PG $\bar{\mathbf{Y}}_n$ and $\alpha_{n,m,j}$ is the j -th element of $\alpha_{n,m}$. λ_j is the j -th regularization parameter defined as

$$\lambda_j = \lambda / (\sqrt{\mathbf{S}_k(j)} + \varepsilon), \quad (5)$$

where $\mathbf{S}_k(j)$ is the j -th singular value of diagonal singular value matrix \mathbf{S}_k (please refer to Eq. (2)) and ε is a small positive number to avoid zero denominator. Noted that $\mathbf{D}_E = \mathbf{U}_k$ if $r = 3p^2$ and $\mathbf{D}_E = \emptyset$ if $r = 0$. The dictionary $\mathbf{D} = [\mathbf{D}_E \ \mathbf{D}_I]$ is orthogonal by checking that:

$$\mathbf{D}^\top \mathbf{D} = \begin{bmatrix} \mathbf{D}_E^\top \\ \mathbf{D}_I^\top \end{bmatrix} [\mathbf{D}_E \ \mathbf{D}_I] = \begin{bmatrix} \mathbf{D}_E^\top \mathbf{D}_E & \mathbf{D}_E^\top \mathbf{D}_I \\ \mathbf{D}_I^\top \mathbf{D}_E & \mathbf{D}_I^\top \mathbf{D}_I \end{bmatrix} = \mathbf{I} \quad (6)$$

We employ an alternating iterative approach to solve the optimization problem (4). Specifically, we initialize the orthogonal dictionary as $\mathbf{D}^{(0)} = \mathbf{U}_k$ and for $t = 0, 1, \dots, T-1$, we alternatively update $\alpha_{n,m}$ and \mathbf{D} as follows:

Updating Sparse Coefficient: Given the orthogonal dictionary $\mathbf{D}^{(t)}$, we update each sparse coding vector $\alpha_{n,m}$ by solving

$$\alpha_{n,m}^{(t)} := \arg \min_{\alpha_{n,m}} \|\bar{\mathbf{y}}_{n,m} - \mathbf{D}^{(t)} \alpha_{n,m}\|_2^2 + \sum_{j=1}^{3p^2} \lambda_j |\alpha_{n,m,j}| \quad (7)$$

Since dictionary $\mathbf{D}^{(t)}$ is orthogonal, the problems (7) has a closed-form solution

$$\alpha_{n,m}^{(t)} = \text{sgn}((\mathbf{D}^{(t)})^\top \bar{\mathbf{y}}_{n,m}) \odot \max(|(\mathbf{D}^{(t)})^\top \bar{\mathbf{y}}_{n,m}| - \lambda, 0), \quad (8)$$

where $\lambda = [\lambda_1, \lambda_2, \dots, \lambda_{3p^2}]$ is the vector of regularization parameter and $\text{sgn}(\bullet)$ is the sign function, \odot means element-wise multiplication. The detailed derivation of Eq. (8) can be found in the supplementary file.

Updating Internal Sub-dictionary: Given the sparse coding vectors $\alpha_{n,m}^{(t)}$, we update the internal sub-dictionary by solving

$$\begin{aligned} \mathbf{D}_I^{(t+1)} &:= \arg \min_{\mathbf{D}_I} \sum_{n=1}^N \sum_{m=1}^M (\|\bar{\mathbf{y}}_{n,m} - \mathbf{D} \alpha_{n,m}^{(t)}\|_2^2) \\ &= \arg \min_{\mathbf{D}_I} \|\mathbf{Y} - \mathbf{D} \mathbf{A}^{(t)}\|_F^2 \end{aligned} \quad (9)$$

$$\text{s.t. } \mathbf{D} = [\mathbf{D}_E \ \mathbf{D}_I], \mathbf{D}_I^\top \mathbf{D}_I = \mathbf{I}_r, \mathbf{D}_E^\top \mathbf{D}_I = \mathbf{0},$$

where $\mathbf{A}^{(t)} = [\alpha_{1,1}^{(t)}, \dots, \alpha_{1,M}^{(t)}, \dots, \alpha_{N,1}^{(t)}, \dots, \alpha_{N,M}^{(t)}]$. The sparse coefficient matrix can be written as $\mathbf{A}^{(t)} = [(\mathbf{A}_E^{(t)})^\top \ (\mathbf{A}_I^{(t)})^\top]^\top$ where the external part $\mathbf{A}_E^{(t)} \in \mathbb{R}^{(3p^2-r) \times NM}$ and the internal part $\mathbf{A}_I^{(t)} \in \mathbb{R}^{r \times NM}$ represent the coding coefficients of \mathbf{Y} over external sub-dictionary \mathbf{D}_E and internal sub-dictionary \mathbf{D}_I , respectively. According to the Theorem 4 in [26], the problem (9) has a closed-form solution $\mathbf{D}_I^{(t+1)} = \mathbf{U}_i \mathbf{V}_i^\top$, where $\mathbf{U}_i \in \mathbb{R}^{3p^2 \times r}$ and $\mathbf{V}_i \in \mathbb{R}^{r \times r}$ are the orthogonal matrices obtained by the following SVD

432 **Alg. 1:** External Prior Guided Internal Prior Learning
 433 for Real Noisy Image Denoising
 434
 435 **Input:** Noisy image \mathbf{y} , external PG prior GMM model
 436 **Output:** The denoised image $\hat{\mathbf{x}}$.
 437 **Initialization:** $\hat{\mathbf{x}}^{(0)} = \mathbf{y}$;
 438 **for** $Ite = 1 : IteNum$ **do**
 439 1. Extracting internal PGs from $\hat{\mathbf{x}}^{(Ite-1)}$;
 440 **for** each PG \mathbf{Y}_n **do**
 441 2. Calculate group mean vector μ_n and form
 442 mean subtracted PG $\bar{\mathbf{Y}}_n$;
 443 3. Subspace selection via Eq. (3);
 444 **end for**
 445 **for** the PGs in each Subspace **do**
 446 4. External PG prior Guided Internal Orthogonal
 447 Dictionary Learning by solving (4);
 448 5. Recover each patch in all PGs via Eq. (11);
 449 **end for**
 450 6. Aggregate the recovered PGs of all subspaces to form
 451 the recovered image $\hat{\mathbf{x}}^{(Ite)}$;
 452 **end for**

$$(\mathbf{I} - \mathbf{D}_e \mathbf{D}_e^\top) \mathbf{Y} (\mathbf{A}_i^{(t)})^\top = \mathbf{U}_i \mathbf{S}_i \mathbf{V}_i^\top. \quad (10)$$

453
 454 The orthogonality of internal dictionary $\mathbf{D}_i^{(t+1)}$ can be
 455 checked by $(\mathbf{D}_i^{(t+1)})^\top (\mathbf{D}_i^{(t+1)}) = \mathbf{V}_i \mathbf{U}_i^\top \mathbf{U}_i \mathbf{V}_i^\top = \mathbf{I}_r$. In Fig. 3 (c) and (d), we illustrate a denoised image by
 456 our proposed method and one internal orthogonal dictionary
 457 learned from PGs of the given noisy image.
 458

3.3. The Denoising Algorithm

463 The denoising of the given noisy image can be simultaneously done with the guided internal dictionary learning
 464 process. Once we obtain the solutions of sparse coding
 465 vectors $\{\hat{\alpha}_{n,m}^{(T-1)}\}$ in Eq. (8) and the orthogonal dictionary
 466 $\mathbf{D}_{(T)} = [\mathbf{D}_E \mathbf{D}_I^{(T)}]$ in Eq. (9), the latent clean patch of a
 467 noisy patch $\hat{\mathbf{y}}_{n,m}$ in PG \mathbf{Y}_n is reconstructed as
 468

$$\hat{\mathbf{y}}_{n,m} = \mathbf{D}_{(T)} \hat{\alpha}_{n,m} + \mu_n, \quad (11)$$

469
 470 where μ_n is the group mean of \mathbf{Y}_n . The latent clean image
 471 is then reconstructed by aggregating all the reconstructed
 472 patches in all PGs. We perform the above denoising pro-
 473 cedures for several iterations for better denoising outputs.
 474 The proposed denoising algorithm is summarized in Alg. 1.
 475 The latent clean image $\hat{\mathbf{x}}$ is reconstructed by aggregating all
 476 the estimated PGs. Similar to [7], we perform the above de-
 477 noising procedures for several iterations for better denoising
 478 outputs. The proposed denoising algorithm is summarized
 479 in Alg. 1.
 480

4. Experiments

482 We evaluate the performance of the proposed algorithm
 483 on real-world noisy images [14, 20] in comparison with
 484

485 state-of-the-art denoising methods [5, 6, 9, 8, 10, 11, 14,
 486 19, 20, 21].
 487

4.1. Implementation Details

488 Our proposed method has two stages: the external prior
 489 learning stage and the external prior guided internal prior
 490 learning stage. In the first stage, we set $p = 6$ (the
 491 patch size), $M = 10$ (the number of similar patches in
 492 a PG), $W = 31$ (the window size for PG searching) and
 493 $K = 32$ (the number of Gaussian components in GMM).
 494 We learn the external GMM prior with 3.6 million PGs ex-
 495 tracted from the Kodak PhotoCD Dataset (<http://r0k.us/graphics/kodak/>), which includes 24 high quality
 496 color images.
 497

498 In the second stage, we set $r = 54$ (the number of atoms
 499 in the external sub-dictionaries); that is, we let the external
 500 sub-dictionary have the same number of atoms as the internal
 501 sub-dictionary to be learned. Our experiments show that
 502 setting r between 27 and 81 will lead to very similar results.
 503 For other parameters, we set $\lambda = 0.001$ (the sparse regu-
 504 larization parameter), $T = 2$ (the number of iterations for
 505 solving problem (4)), and $IteNum = 4$ (the number of iter-
 506 ations for Alg.1). All parameters of our method are fixed to
 507 all experiments, which are run under the Matlab2014b en-
 508 vironment on a machine with Intel(R) Core(TM) i7-5930K
 509 CPU of 3.5GHz and 32GB RAM.
 510

4.2. The Testing Datasets

511 We evaluate the proposed method on two real noisy im-
 512 age datasets, where the images were captured under indoor
 513 or outdoor lighting conditions by different types of cameras
 514 and camera settings.
 515

516 The first dataset is provided in [20], which includes 20
 517 real noisy images collected under uncontrolled outdoor en-
 518 vironment. Since there is no “ground truth” of the noisy
 519 images, the objective measures such as PSNR cannot be
 520 computed on this dataset.
 521

522 The second dataset is provided in [14], which includes
 523 noisy images of 17 static scenes. The noisy images were
 524 collected under controlled indoor environment. Each scene
 525 was shot 500 times under the same camera and camera set-
 526 ting. The mean image of the 500 shots is roughly taken as
 527 the “ground truth”, with which the PSNR can be computed.
 528 Since the image size is very large (about 7000×5000) and
 529 the 17 scenes share repetitive contents, the authors of [14]
 530 cropped 15 smaller images (of size 512×512) to perform
 531 experiments. To more comprehensively evaluate the pro-
 532 posed methods, we cropped 60 images of size 500×500
 533 from the dataset for experiments. Some samples are shown
 534 in Fig. 3. Note that the noise in our cropped 60 images
 535 is different from the noise in the 15 images cropped by the
 536 authors of [14] since they are from different shots.
 537



Figure 3. Some samples cropped from real noisy images of [14].
Table 1. Average PSNR (dB) results and Run Time (seconds) of the External, the Internal, and our proposed methods on 60 real noisy images (of size $500 \times 500 \times 3$) cropped from [14].

	Noisy	External	Internal	Guided Internal
PSNR	34.51	38.21	38.07	38.75
Time	—	39.57	667.36	41.89

4.3. Comparison among external, internal and guided internal priors

To demonstrate the advantages of external prior guided internal priors, in this section we perform real noisy image denoising by using external priors (denoted by “External”), internal priors (denoted by “Internal”), and the proposed guided internal priors (denoted by “Guided Internal”), respectively. For the “External” method, we utilize the full external dictionaries (i.e., $r = 108$ in Eq. (4)) for denoising. For the “Internal” method, the overall framework is similar to the method of [3]. A GMM model (with $K = 32$ Gaussians) is directly learned from the PGs extracted from the given noisy image without using any external data, and then the internal orthogonal dictionary is obtained via Eqn. (2) to perform denoising. All parameters of the “External” and “Internal” methods are tuned to achieve their best performance.

We compare the three methods mentioned above on the 60 cropped images from [14]. The average PSNR and run time are listed in Table 1. It can be seen that “Guided Internal” prior achieves better PSNR than both “External” and “Internal” priors. In addition, the “Internal” method is very slow because it involves online GMM learning, while the “Guided Internal” method is only a little slower than the “External” method. Fig. 4 and Fig. 5 show the denoised images of two noisy image by the three methods. We can see that the “External” method is good at recovering large-scale structures (see Fig. 4) while the “Internal” method is good at recovering fine-scale textures (see Fig. 5). By utilizing external priors to guide the internal prior learning, our proposed method can effectively recover both the large-scale structures and fine-scale textures.

4.4. Comparison with State-of-the-Art Denoising Methods

We compare the proposed method with state-of-the-art image denoising methods, including CBM3D [5, 6], WNNM [8], MLP [9], CSF [10], TNRD [11], Noise Clinic (NC) [19], Cross-Channel (CC) [14], and Neat Image (NI) [21]. Among them, CBM3D, WNNM, MLP, CSF and

TNRD are designed based on Gaussian noise model, and they need to know the noise level for denoising. We use the method in [27] to estimate the noise level for them. All the other parameters in these methods are set as the default ones. Since WNNM, MLP, CSF and TNRD are designed for grayscale images, we use them to denoise the R, G, B channels separately for color noisy images.

Like our method, the NC is a blind image denoising method which does not need any noise prior. The NI is a commercial software for image denoising, which has been embedded into Photoshop and Corel PaintShop [21]. The code of CC is not released but its results on the 15 cropped images are available at [14]. Therefore, we only compare with it on the 15 cropped images from [14].

4.4.1 Results on Dataset [20]

Since there is no “ground truth” for the real noisy images in dataset [20], we only compare the visual quality of the denoised images by different methods. (Note that method CC [14] is not compared since its code is not available.) Fig. 7 shows the denoised images of “Dog”. It can be seen that CBM3D and WNNM tend to over-smooth much the image while remaining some noise caused color artifacts. MLP and TNRD are likely to remain many noise-caused color artifacts across the whole image. These results demonstrate that the methods designed with Gaussian noise model are not effective for real noise removal. Though NC and NI methods are specifically developed for real noisy images, their performance on noise removal is not very satisfactory. In comparison, our proposed method recovers much better the structures and textures (such as the eye area) than the other competing methods. More visual comparisons on dataset [20] can be found in the supplementary file.

4.4.2 Comparison on Dataset [14]

As described in section 4.2, there is a mean image for each of the 17 scenes used in dataset [14], and those mean images can be roughly taken as “ground truth” images for quantitative evaluation of denoising algorithms. We firstly perform quantitative comparison on the 15 cropped images used in [14]. The PSNR results of CBM3D [5], WNNM [8], MLP [9], CSF [10], TNRD [11], NC [19] and CC [14] are listed in Table 2. (The results of CC are copied from the original paper [14].) The best PSNR result of each image is highlighted in bold. One can see that on 9 out of the 15 images, our method achieves the best PSNR values. CC achieves the best PSNR on 3 of the 15 images. It should be noted that in the CC method, a specific model is trained for each camera and camera setting, while our method uses the same model for all images. On average, our proposed method has 0.28dB PSNR improvements over [14] and much higher PSNR gains over other competing methods. Fig. 6 shows

594
595
596
597
598
599
600
601
602
603
604
605
606
607
608
609
610
611
612
613
614
615
616
617
618
619
620
621
622
623
624
625
626
627
628
629
630
631
632
633
634
635
636
637
638
639
640
641
642
643
644
645
646
647

648
649
650
651
652
653
654
655
656

Figure 4. Denoised images of the 96-th cropped image from “Nikon D600 ISO 3200 C1” [14] by different methods. The images are better to be zoomed in on screen.

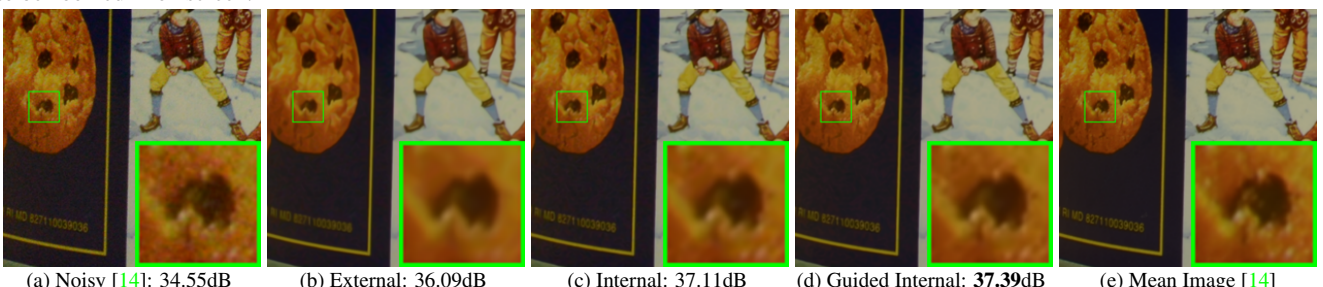
657
658
659
660
661
662
663
664
665
666
667

Figure 5. Denoised images of the 94-th cropped image from “Nikon D600 ISO 3200 C1” [14] by different methods. The images are better to be zoomed in on screen.

671
672
673
674
675
676
677
678
679

the denoised images of a scene captured by Canon 5D Mark 3 at ISO = 3200. We can see that CBM3D, WNNM, NC, NI, and CC would either remain noise or generate artifacts, while MLP, TNRD over-smooth much the image. By using the external prior guided internal priors, our proposed method preserves edges and textures better than other methods, leading to visually pleasant outputs. More visual comparisons can be found in the supplementary file.

680
681
682
683
684
685
686
687
688
689
690
691
692
693
694
695
696
697
698
699
700
701

The real noisy images in the second dataset [14] have corresponding “ground truth” images. On this dataset, we firstly perform comparison on the 15 cropped images used in [14]. The compared method are BM3D [5], WNNM [8], MLP [9], CSF [10], TRD [11], Noise Clinic (NC) [19], and Cross-Channel (CC) [14]. The PSNR values are listed in Table 2. As we can see, on most (9 out of the 15) images captured by different cameras and camera settings, our proposed method obtains better PSNR values than the other methods. Noted that, though in [14] a specific model is trained for each camera and camera setting, our proposed general method still gains 0.28dB improvements on PNSR over [14]. We also compare the visual quality of the denoised images by the competing methods. Fig. 7 shows the denoised images of a scene captured by Canon 5D Mark 3 at ISO = 3200 by the competing methods. More visual comparisons can be found in the supplementary file. We can see that BM3D, WNNM, NC, NI, and CC would either remain noise or generate artifacts, while MLP, TRD are likely to over-smooth the image. By combining the external and internal priors, our proposed method preserves edges and textures better than other methods.

To evaluate the compared methods on more samples, we then perform denoising experiments on the 60 smaller images cropped from the 17 images provided in [14]. The average PSNR results are listed in Table 3 (the code of [14] is not available so that it is not compared). The numbers in red color and blue color are the best and second best results, respectively. It can be seen that our proposed method achieves much better PSNR results than the other methods. The improvement of our method over the second best method (TRD) is 1dB. Due to the spacial limitations, the visual comparisions are provided in the supplementary file.

5. Conclusion and Future Work

Image priors are important for solving image denoising problems. The external priors learned from external clean images are generally effective to most images, while the internal priors learned directly from the noisy image are adaptive to the given image but would be biased by the complex noise in real noisy images. In this paper, we demonstrates that, once unifying both the priors in external clean images and internal noisy images, we can achieve much better while still efficient performance on real image denoising problem. Specifically, the external patch group (PG) priors learned on natural clean images can be used to guide the subspace selection and orthogonal dictionary learning of internal noisy PGs from given noisy images. The experiments on real image denoising problem have demonstrated the powerful ability of the proposed method. In the future, we will speed up the proposed algorithm and evaluate the proposed method on other computer vision tasks such as

702
703
704
705
706
707
708
709
710
711
712
713
714
715
716
717
718
719
720
721
722
723
724
725
726
727
728
729
730
731
732
733
734
735
736
737
738
739
740
741
742
743
744
745
746
747
748
749
750
751
752
753
754
755

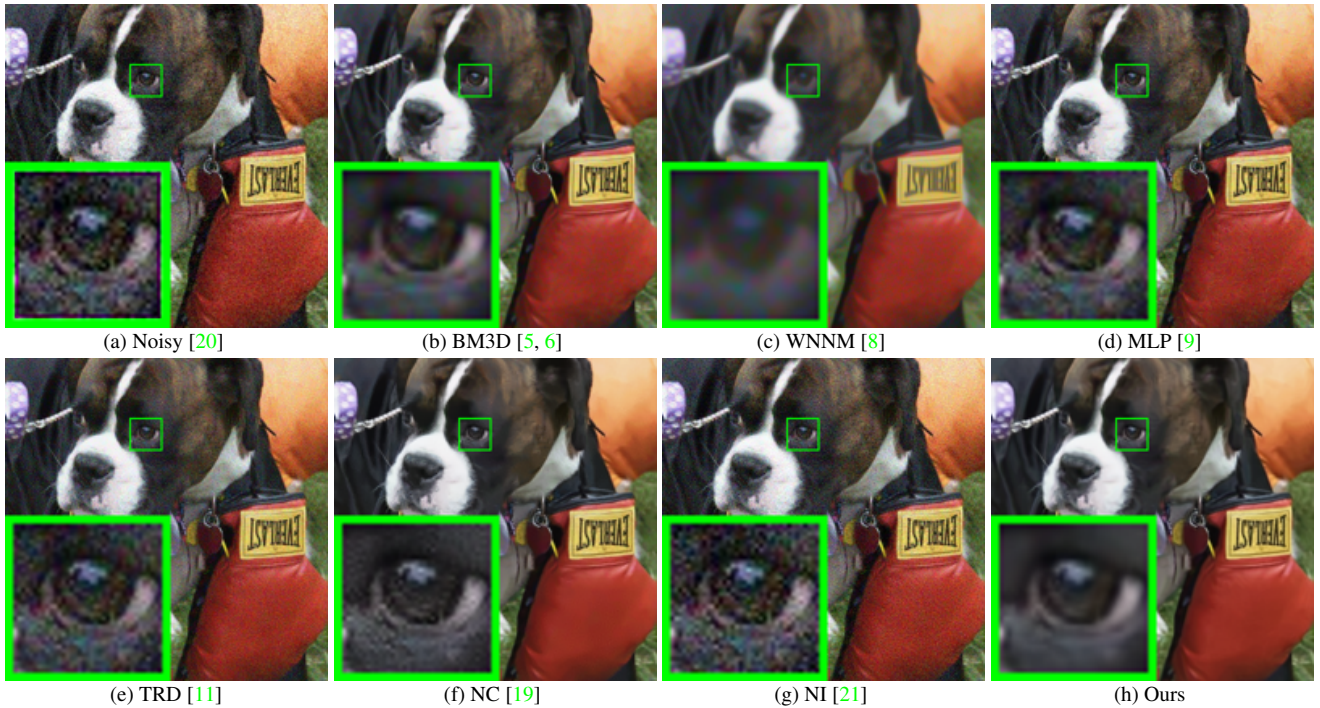


Figure 6. Denoised images of the image “Dog” by different methods. The images are better to be zoomed in on screen.

Table 2. Average PSNR(dB) results of different methods on 15 cropped real noisy images used in [14].

Camera Settings	Noisy	BM3D	WNNM	MLP	CSF	TRD	NI	NC	CC	Ours
Canon 5D Mark III ISO = 3200	37.00	37.08	37.09	33.92	35.68	36.20	37.68	38.76	38.37	40.50
	33.88	33.94	33.93	33.24	34.03	34.35	34.87	35.69	35.37	37.05
	33.83	33.88	33.90	32.37	32.63	33.10	34.77	35.54	34.91	36.11
Nikon D600 ISO = 3200	33.28	33.33	33.34	31.93	31.78	32.28	34.12	35.57	34.98	34.88
	33.77	33.85	33.79	34.15	35.16	35.34	35.36	36.70	35.95	36.31
	34.93	35.02	34.95	37.89	39.98	40.51	38.68	39.28	41.15	39.23
Nikon D800 ISO = 1600	35.47	35.54	35.57	33.77	34.84	35.09	37.34	38.01	37.99	38.40
	35.71	35.79	35.77	35.89	38.42	38.65	38.57	39.05	40.36	40.92
	34.81	34.92	34.95	34.25	35.79	35.85	37.87	38.20	38.30	38.97
Nikon D800 ISO = 3200	33.26	33.34	33.31	37.42	38.36	38.56	36.95	38.07	39.01	38.66
	32.89	32.95	32.96	34.88	35.53	35.76	35.09	35.72	36.75	37.07
	32.91	32.98	32.96	38.54	40.05	40.59	36.91	36.76	39.06	38.52
Nikon D800 ISO = 6400	29.63	29.66	29.71	33.59	34.08	34.25	31.28	33.49	34.61	33.76
	29.97	30.01	29.98	31.55	32.13	32.38	31.38	32.79	33.21	33.43
	29.87	29.90	29.95	31.42	31.52	31.76	31.40	32.86	33.22	33.58
Average	33.41	33.48	33.48	34.32	35.33	35.65	35.49	36.43	36.88	37.16

Table 3. Average PSNR(dB) results of different methods on 60 real noisy images cropped from [14].

Methods	BM3D	WNNM	MLP	CSF
PSNR	34.58	34.52	36.19	37.40
Methods	TRD	NI	NC	Ours
PSNR	37.75	36.53	37.57	38.75

image super-resolution.

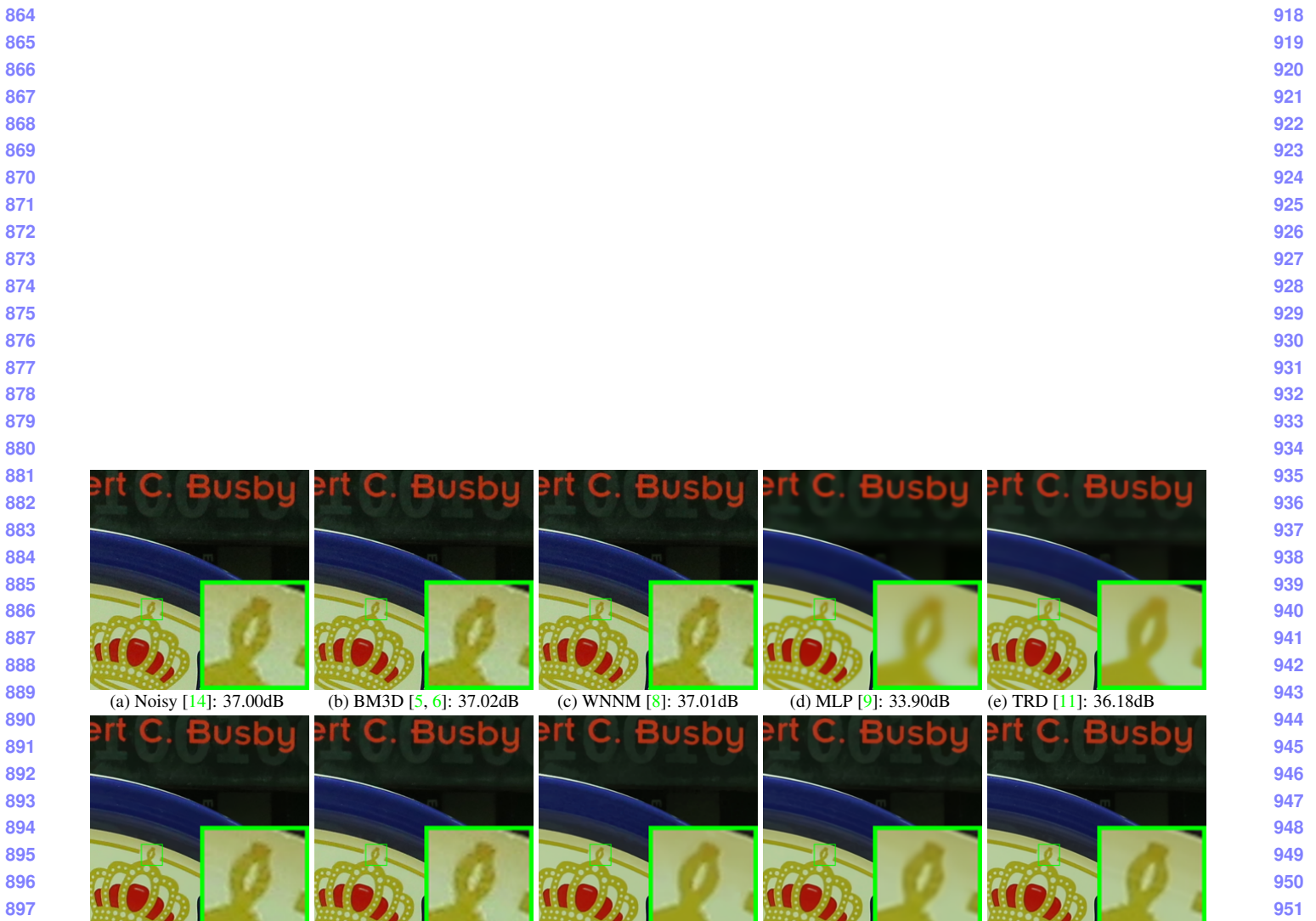


Figure 7. Denoised images of the image “Canon 5D Mark 3 ISO 3200 1” by different methods. The images are better to be zoomed in on screen.

972

References

973

974

975

976

977

978

979

980

981

982

983

984

985

986

987

988

989

990

991

992

993

994

995

996

997

998

999

1000

1001

1002

1003

1004

1005

1006

1007

1008

1009

1010

1011

1012

1013

1014

1015

1016

1017

1018

1019

1020

1021

1022

1023

1024

1025

- [1] M. Elad and M. Aharon. Image denoising via sparse and redundant representations over learned dictionaries. *IEEE Transactions on Image Processing*, 15(12):3736–3745, 2006. [1](#), [2](#)
- [2] J. Mairal, F. Bach, J. Ponce, G. Sapiro, and A. Zisserman. Non-local sparse models for image restoration. *IEEE International Conference on Computer Vision (ICCV)*, pages 2272–2279, 2009. [1](#)
- [3] W. Dong, L. Zhang, G. Shi, and X. Li. Nonlocally centralized sparse representation for image restoration. *IEEE Transactions on Image Processing*, 22(4):1620–1630, 2013. [1](#), [2](#), [6](#)
- [4] A. Buades, B. Coll, and J. M. Morel. A non-local algorithm for image denoising. *IEEE Conference on Computer Vision and Pattern Recognition (CVPR)*, pages 60–65, 2005. [1](#)
- [5] K. Dabov, A. Foi, V. Katkovnik, and K. Egiazarian. Image denoising by sparse 3-D transform-domain collaborative filtering. *IEEE Transactions on Image Processing*, 16(8):2080–2095, 2007. [1](#), [2](#), [5](#), [6](#), [8](#), [9](#)
- [6] K. Dabov, A. Foi, V. Katkovnik, and K. Egiazarian. Color image denoising via sparse 3D collaborative filtering with grouping constraint in luminance-chrominance space. *IEEE International Conference on Image Processing (ICIP)*, pages 313–316, 2007. [1](#), [2](#), [5](#), [6](#), [8](#), [9](#)
- [7] J. Xu, L. Zhang, W. Zuo, D. Zhang, and X. Feng. Patch group based nonlocal self-similarity prior learning for image denoising. *IEEE International Conference on Computer Vision (ICCV)*, pages 244–252, 2015. [1](#), [2](#), [3](#), [5](#)
- [8] S. Gu, L. Zhang, W. Zuo, and X. Feng. Weighted nuclear norm minimization with application to image denoising. *IEEE Conference on Computer Vision and Pattern Recognition (CVPR)*, pages 2862–2869, 2014. [1](#), [2](#), [5](#), [6](#), [8](#), [9](#)
- [9] H. C. Burger, C. J. Schuler, and S. Harmeling. Image denoising: Can plain neural networks compete with BM3D? *IEEE Conference on Computer Vision and Pattern Recognition (CVPR)*, pages 2392–2399, 2012. [1](#), [2](#), [5](#), [6](#), [8](#), [9](#)
- [10] U. Schmidt and S. Roth. Shrinkage fields for effective image restoration. *IEEE Conference on Computer Vision and Pattern Recognition (CVPR)*, pages 2774–2781, June 2014. [1](#), [2](#), [5](#), [6](#)
- [11] Y. Chen, W. Yu, and T. Pock. On learning optimized reaction diffusion processes for effective image restoration. *IEEE Conference on Computer Vision and Pattern Recognition (CVPR)*, pages 5261–5269, 2015. [1](#), [2](#), [5](#), [6](#), [8](#), [9](#)
- [12] S. Roth and M. J. Black. Fields of experts. *International Journal of Computer Vision*, 82(2):205–229, 2009. [1](#), [2](#)
- [13] D. Zoran and Y. Weiss. From learning models of natural image patches to whole image restoration. *IEEE International Conference on Computer Vision (ICCV)*, pages 479–486, 2011. [1](#), [2](#), [3](#)

- [14] S. Nam, Y. Hwang, Y. Matsushita, and S. J. Kim. A holistic approach to cross-channel image noise modeling and its application to image denoising. *IEEE Conference on Computer Vision and Pattern Recognition (CVPR)*, pages 1683–1691, 2016. [1](#), [2](#), [5](#), [6](#), [7](#), [8](#), [9](#) [1026](#)
- [15] G. E Healey and R. Kondepudy. Radiometric CCD camera calibration and noise estimation. *IEEE Transactions on Pattern Analysis and Machine Intelligence*, 16(3):267–276, 1994. [1](#) [1027](#)
- [16] C. Liu, R. Szeliski, S. Bing Kang, C. L. Zitnick, and W. T. Freeman. Automatic estimation and removal of noise from a single image. *IEEE Transactions on Pattern Analysis and Machine Intelligence*, 30(2):299–314, 2008. [1](#), [2](#) [1035](#)
- [17] Z. Gong, Z. Shen, and K.-C. Toh. Image restoration with mixed or unknown noises. *Multiscale Modeling & Simulation*, 12(2):458–487, 2014. [1](#), [2](#) [1040](#)
- [18] F. Zhu, G. Chen, and P.-A. Heng. From noise modeling to blind image denoising. *IEEE Conference on Computer Vision and Pattern Recognition (CVPR)*, June 2016. [1](#), [2](#) [1042](#)
- [19] M. Lebrun, M. Colom, and J.-M. Morel. Multiscale image blind denoising. *IEEE Transactions on Image Processing*, 24(10):3149–3161, 2015. [1](#), [2](#), [5](#), [6](#), [8](#), [9](#) [1045](#)
- [20] M. Lebrun, M. Colom, and J. M. Morel. The noise clinic: a blind image denoising algorithm. <http://www.ipol.im/pub/art/2015/125/>. Accessed 01 28, 2015. [1](#), [2](#), [5](#), [6](#), [8](#) [1051](#)
- [21] Neatlab ABSoft. Neat Image. <https://ni.neatvideo.com/home>. [1](#), [2](#), [5](#), [6](#), [8](#), [9](#) [1053](#)
- [22] G. Yu, G. Sapiro, and S. Mallat. Solving inverse problems with piecewise linear estimators: From Gaussian mixture models to structured sparsity. *IEEE Transactions on Image Processing*, 21(5):2481–2499, 2012. [2](#) [1056](#)
- [23] M. Zontak and M. Irani. Internal statistics of a single natural image. *IEEE Conference on Computer Vision and Pattern Recognition (CVPR)*, pages 977–984, 2011. [2](#) [1059](#)
- [24] M. Lebrun, A. Buades, and J. M. Morel. A nonlocal Bayesian image denoising algorithm. *SIAM Journal on Imaging Sciences*, 6(3):1665–1688, 2013. [2](#) [1064](#)
- [25] D. L. Donoho and X. Huo. Uncertainty principles and ideal atomic decomposition. *IEEE Transactions on Information Theory*, 47(7):2845–2862, 2001. [4](#) [1066](#)
- [26] H. Zou, T. Hastie, and R. Tibshirani. Sparse principal component analysis. *Journal of Computational and Graphical Statistics*, 15(2):265–286, 2006. [4](#) [1069](#)
- [27] X. Liu, M. Tanaka, and M. Okutomi. Single-image noise level estimation for blind denoising. *IEEE transactions on Image Processing*, 22(12):5226–5237, 2013. [6](#) [1073](#)